Polymer 50 (2009) 2424–2435

Contents lists available at ScienceDirect

Polymer

journal homepage: www.elsevier.com/locate/polymer

Dynamics of concentrated solutions of low molecular weight phenolics and poly(2-vinylpyridine): Role of intermolecular hydrogen bonding

Pornpen Atorngitjawat [1], Robert J. Klein [2], Amanda G. McDermott, Kevin A. Masser, Paul C. Painter, James Runt*

Department of Materials Science and Engineering, The Pennsylvania State University, University Park, PA 16802, USA

ARTICLE INFO

Article history:
Received 18 November 2008
Received in revised form
9 February 2009
Accepted 15 February 2009
Available online 19 March 2009

Keywords:
Dynamics
Dielectric relaxation spectroscopy
Polymer mixtures

ABSTRACT

The molecular dynamics of solutions of poly(2-vinylpyridine) (P2VPy) and a series of low molecular weight phenols containing from one to six hydroxyl groups were investigated using broadband dielectric spectroscopy (DRS). Dynamic mechanical analysis, Fourier transform infrared spectroscopy, differential scanning calorimetry, small-angle X-ray scattering and wide-angle X-ray diffraction were employed in a complementary role. Segmental relaxation times for the α processes of all solutions follow expectations from T_gs derived from DSC experiments. For three of the model mixtures at 30 and 50 mol% [i.e., those containing bis (4-hydroxyphenyl) methane, 2,6 dihydroxynaphthalene, and 2,2-methylenebis[6-(2-hydroxy-5-methylbenzyl)-*p*-cresol] significantly broadened dielectric α relaxation time distributions were observed, indicating dynamic heterogeneity. On the other hand, 4-ethyphenol–P2VPy solutions display dynamic homogeneity. P2VPy with 10 mol% 2,3,3,4,4,5-hexahydroxybenzophenone behaved differently than all mixtures investigated in this study: it displayed a T_g (and T_α) significantly higher than that of the neat components, a small SAXS scattering peak, and an additional dielectric relaxation that we propose originates from Maxwell–Wagner–Sillars interfacial polarization. We propose that this behavior is a result of a phase separation of different types of hydrogen-bonded complexes, one rich in P2VPy and the other involving the type of 2,3,3,4,4,5-hexahydroxybenzophenone hydrogen-bonded structures found in the neat state. Intermolecular hydrogen bonding in all of the P2VPy–phenol mixtures suppresses, in some cases completely, the local P2VPy β relaxation by decreasing the mobility of the pyridine side groups.

1. Introduction

The associative interactions of the hydrogen bond have been of key interest for many years and have been widely studied. Intermolecular hydrogen bonding is well known to have an important effect on the miscibility of polymer blends and polymer–small molecule mixtures [1–15], damping concentration fluctuations and coupling the components' segmental relaxations. Hydrogen bonds serve as 'stickers' and the blend (or solution) can be considered a transient network. Supramolecular assemblies [16–18] and polymer complexes [19–22] can be also created through strong intermolecular hydrogen bonds.

The investigation of the influence of small molecules ("plasticizers" or "anti-plasticizers") on the mobility of concentrated polymer mixtures has practical importance in a number of areas, including mechanical behavior and mobility (and permeability) of small molecules in the glassy state. For example, intercomponent hydrogen bonding in P2VPy [and poly(methyl methacrylate)] – silica nanocomposites was found to lead to an increase T_g and suppression of physical aging in glassy state [23,24]. Hydrogen bonding is also intimately involved in the anti-plasticizing effect of glycerol on trehalose, leading to a significant increase in preservation times for proteins stored in such formulations [25].

Investigations of intermolecular coupling on the dynamics of polymers mixtures have frequently used dielectric spectroscopy. A dielectric relaxation associated with transient hydrogen bonds in polyisobutylene modified with urazoylbenzoic acid groups [26,27], in supramolecular assemblies composed of small molecules linked with hydrogen bonds [17], and in sulfonic acid modified polystyrene [28] have been observed at temperatures above the segmental α process. In addition, it has been found that the local dielectric β process can be suppressed in blends when strong intermolecular hydrogen bonding is present [12–14]. Intermolecular hydrogen

* Corresponding author.
E-mail address: runt@matse.psu.edu (J. Runt).
[1] Present address: Faculty of Science, Burapha University, Thailand.
[2] Present address: Luna Innovations, Charlottesville, VA, USA.

0032-3861/$ – see front matter © 2009 Elsevier Ltd. All rights reserved.
doi:10.1016/j.polymer.2009.02.049

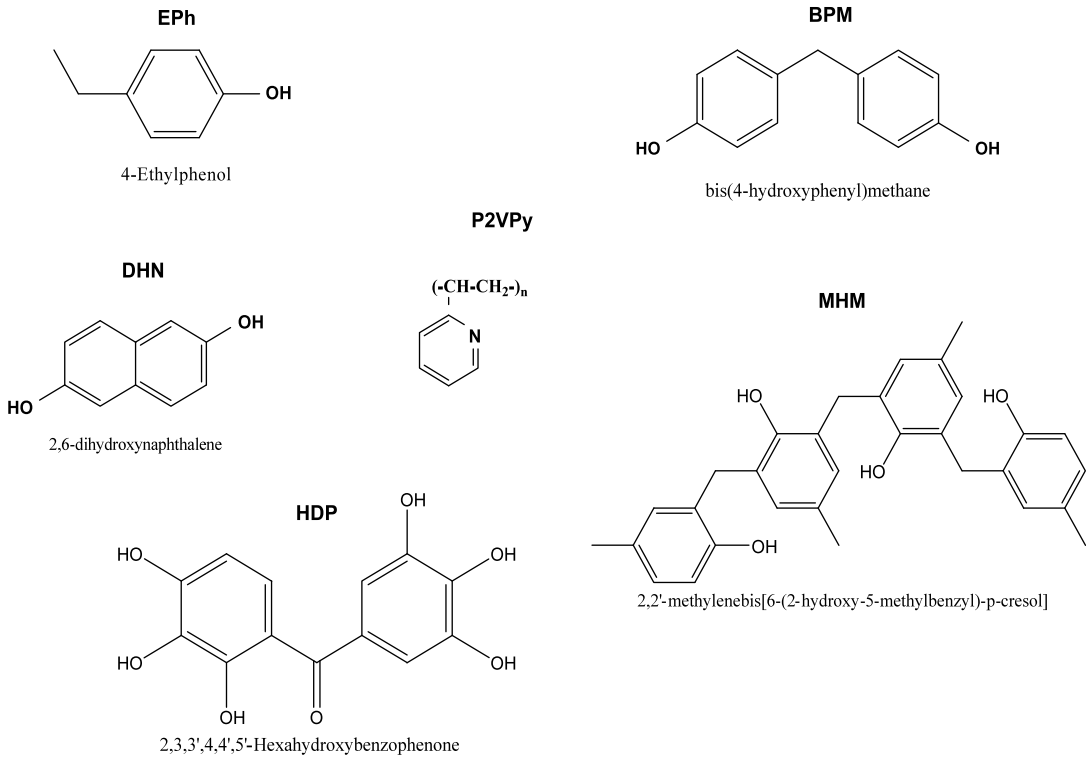

Fig. 1. Chemical structures of P2VPy, EPh, BPM, DHN, MHM and HDP.

bonds have also been observed to slow down relaxation times and increase the fragility of the segmental α process in polymer blends [13–15].

In the present study we explore the effects of addition of low molecular weight phenols (containing from one to six hydroxyl groups) on the dynamics of a host polymer. Poly(2-vinyl pyridine) (P2VPy) was chosen for this study because of the proton acceptor ability of the pyridine pendant group, facilitating the formation of hydrogen bonds with proton donor molecules [16,22,29–32].

2. Experimental

2.1. Materials and sample preparation

Poly(2-vinylpyridine) (P2VPy) with $M_w \sim 100{,}000$ was purchased from Scientific Polymer Products. Bis (4-hydroxyphenyl) methane (BPM), 2,6 dihydroxynaphthalene (DHN), and 4-ethyphenol (EPh) were obtained from Aldrich. 2,2-methylene bis [6-(2-hydroxy-5-methylbenzyl)-*p*-cresol] (MHM) and 2,3,3,4,4,5-hexahydroxybenzophenone (HDP) were purchased from TCI, America. The structures of these hydroxyl-containing molecules are provided in Fig. 1 and their glass transitions, melting temperatures and calculated dipole moments are provided in Table 1. T_gs in Table 1 were estimated from $T_g = T_m/1.3$ [12], since they could not be determined directly due to extensive crystallization of the small molecules on cooling. All but DHN can be considered plasticizers for P2VPy, as their estimated T_gs are lower than P2VPy, but only DHP ($T_g \sim 28$ °C) and EPh ($T_g \sim -28$ °C) have very significantly different intrinsic mobilities compared to P2VPy ($T_g \sim 107$ °C).

Dipole moments of the VPy monomer and small molecules were determined using quantum chemical calculations performed using Gaussian 03 [33]. Geometry optimizations were carried out both using density functional theory (DFT) with the B3LYP functional

Table 1
Estimated glass transition temperatures, experimental melting points and calculated dipole moments for EPh, BPM, DHN, MHM, and HDP.

Material	Estimated T_g (°C)	T_m (°C)	Calculated dipole moment (D)
P2VPy	107	–	1.95
EPh	−28	45	1.50
BPM	62	162	3.09
DHN	110	225	0.001
MHM	74	178	4.90
HDP	28	115	7.23

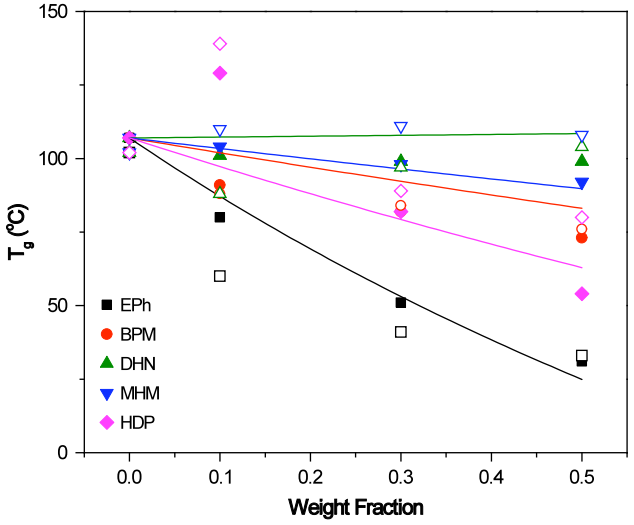

Fig. 2. Glass transition temperatures for P2VPy mixtures as a function of weight fraction of small molecules. Solid and unfilled symbols are T_gs obtained from DSC and DRS, respectively. Solid lines indicate the T_gs estimated from the Fox equation.

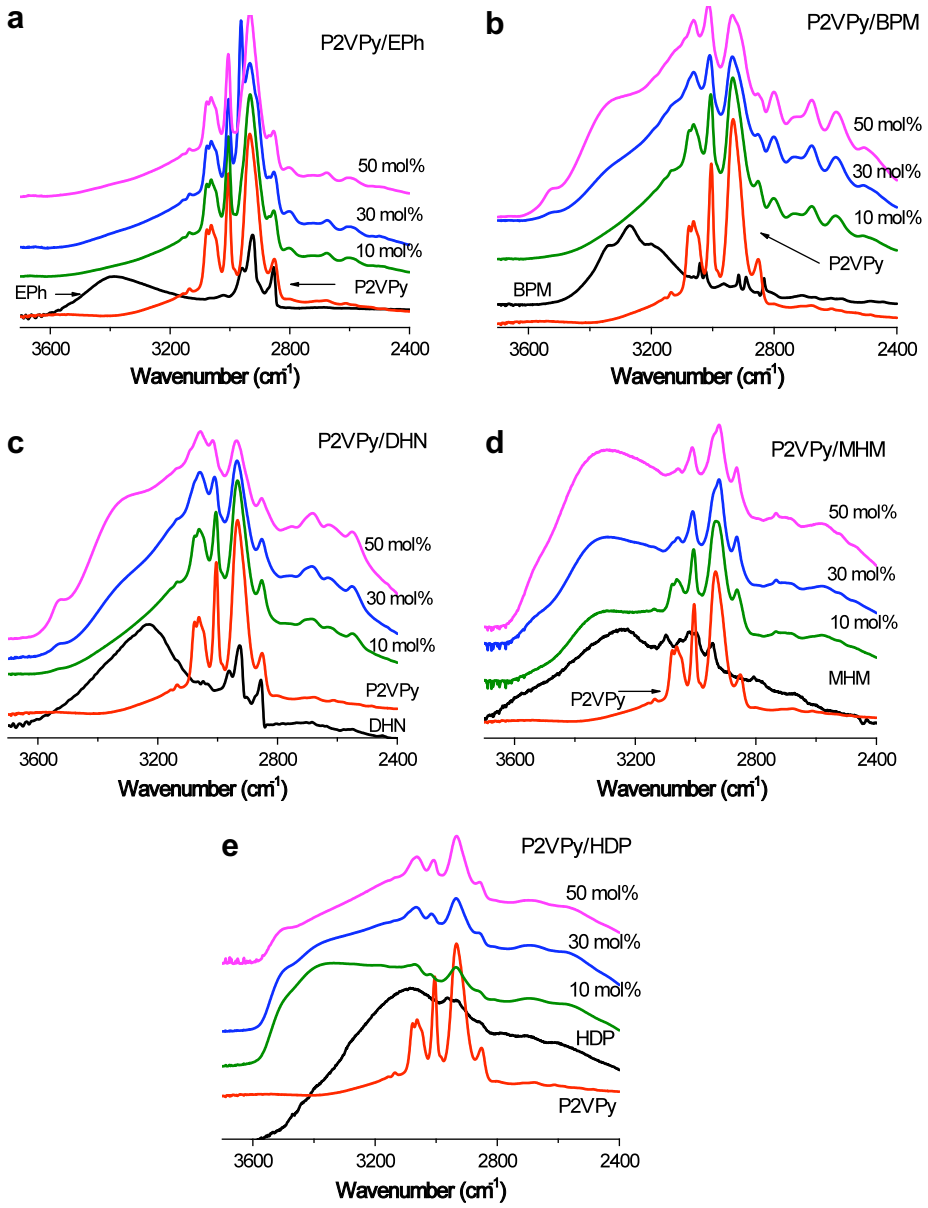

Fig. 3. FTIR spectra of P2VPy mixed with (a) EPh (b) BPM (c) DHN (d) MHM and (e) HDP at 10, 30 and 50 mol%.

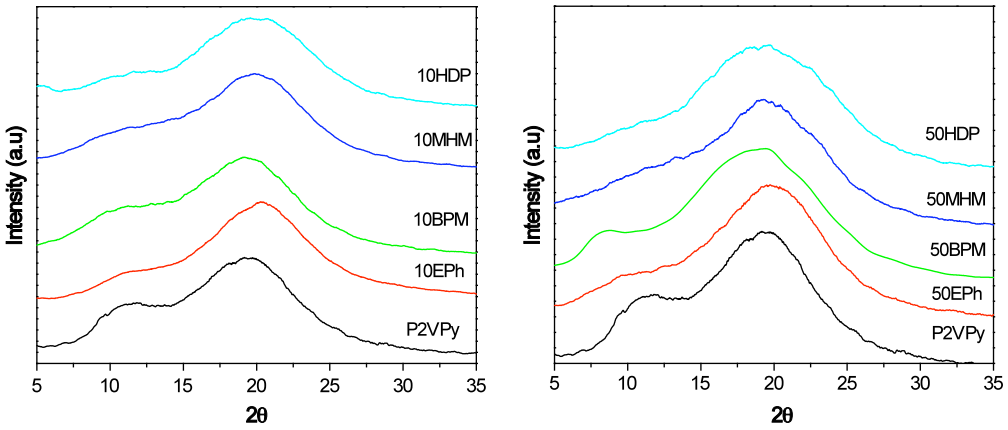

Fig. 4. WAXD patterns of P2VPy mixtures containing 10 and 50 mol% phenolic diluents.

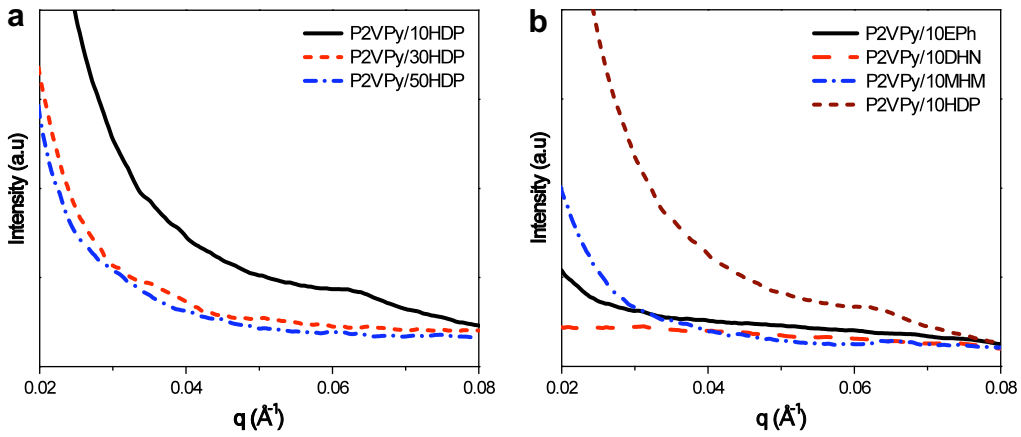

Fig. 5. SAXS profiles of (a) P2VPy/HDP at 10, 30 and 50 mol% of HDP and (b) P2VPy mixed with 10 mol% of EPh, DHN, MHM and HDP.

and via Møller–Plesset (MP2) calculations. The values from both approaches agree quite well, and the values displayed in Table 1 are those from DFT. Note that these values are essentially gas phase moments at 0 K. For the two cases where dipole moments are reported in the literature, the calculated values agree very well with the moments measured in benzene solution (i.e., VPy = 2.04 D at 25 °C [34] and EPh = 1.58 at 27 °C [34] and, in a separate publication = 1.78 at 30 °C [35]). The near-zero magnitude obtained for DHN is consistent with its planar and rotationally symmetric geometry, although this may not persist in the liquid phase.

P2VPy/BPM, P2VPy/DHN, and P2VPy/EPh mixtures were prepared by mixing (with stirring) P2VPy in methanol with 10, 30 and 50 mol% of BPM, DHN, and EPh in methanol for 24 h. P2VPy/MHM and P2VPy/HDP mixtures were prepared by mixing P2VPy with MHM and HDP in DMF. All concentrated polymer solutions were prepared in film form by evaporating the respective solvent. Films were heated to 120 °C under vacuum for 24 h to remove solvent and water.

2.2. Differential scanning calorimetry (DSC)

Glass transition temperatures (T_g) were determined using a TA Instruments Q100 DSC. Temperature was calibrated using an indium standard. The sample films were cut and weighed from 7 to 10 mg. Samples were first heated from 40 °C to 150 °C at a heating rate of 10 °C/min, and cooled at 40 °C/min to 30 °C. Samples were held at 30 °C for 5 min, and then reheated to 200 °C at a heating rate of 10 °C/min. Results shown in this paper are taken from the last step.

2.3. Fourier transform infrared spectroscopy (FTIR)

Infrared spectra were obtained using a Bio-Rad FTS-6 spectrometer, signal averaging 128 scans at a resolution of 2 cm^{-1}. Samples were prepared by depositing sample solutions on KBr windows and the solvent evaporated at room temperature, followed by gradually heating to 120 °C, and then maintaining at 120 °C under vacuum for 24 h.

2.4. Wide-angle X-ray diffraction (WAXD)

WAXD patterns were acquired using a Scintag Pad V diffractometer, operated with CuKα radiation ($\lambda = 0.154$ nm) at 35 kV and 30 mA. The sample films were scanned continuously at a scanning rate of 2°/min and over a 2θ range from 5 to 40°.

2.5. Small-angle X-ray scattering (SAXS)

The SAXS profiles were collected on a molecular metrology SAXS instrument using a CuKα radiation source ($\lambda = 0.154$ nm) and a two-dimensional multi-wire detector. The scattering vector (q) was calibrated with silver behenate. A parallel ionization detector was placed in front of the samples to record the incident and transmitted intensities. The sample to detector distance was 1.5 m. Data were acquired for 2 h and azimuthally averaged to yield a one dimensional profile of intensity I(q) vs. scattering vector q ($q = (4\pi/\lambda)\sin\theta$, where λ is the X-ray wavelength and 2θ is the scattering angle).

2.6. Dynamic mechanical analysis (DMA)

Dynamic mechanical properties in tensile mode were acquired using a TA Q-800 DMA, at a frequency of 1 Hz and a heating rate of 5 °C/min. The storage (E′) and loss moduli (E″) were determined as a function of temperature (from 50 to 200 °C) for rectangular films (18 mm × 5 mm × 0.1–0.3 mm).

2.7. Broadband dielectric relaxation spectroscopy (DRS)

Dielectric relaxation spectra were collected isothermally using a Novocontrol GmbH Concept 40 broadband dielectric spectrometer in the frequency domain from 0.01 Hz to 1 MHz in the range of −60 °C–190 °C. Temperature stability was controlled within ±0.2 °C. Sample films were sputtered with gold, covered by silver sheets and tightly sandwiched between electrodes of 2 cm diameter.

2.7.1. Data processing

The relaxation time τ_{max} and dielectric relaxation strength $\Delta\varepsilon$ were obtained by fitting the isothermal dielectric loss $\varepsilon''(f)$ curves with the Havriliak–Negami (HN) function. The sum of multiple HN functions and a dc loss contribution were used to fit the experimental loss curves [36]:

$$\varepsilon^*(\omega) = \varepsilon'(\omega) - i\varepsilon''(\omega) = \varepsilon_\infty - i\frac{\sigma_0}{(\varepsilon_0\omega)^s} + \sum \frac{\Delta\varepsilon}{\left[1 + (i\tau_{HN}\omega)^m\right]^n} \quad (1)$$

where ε^*, ε', and ε'' are the complex, real and imaginary components of the dielectric permittivity, respectively; the relaxation strength $\Delta\varepsilon = \varepsilon_\infty - \varepsilon_s$, where ε_∞ and ε_s are the dielectric constants at limiting high and low frequencies, respectively; σ_0 is the dc

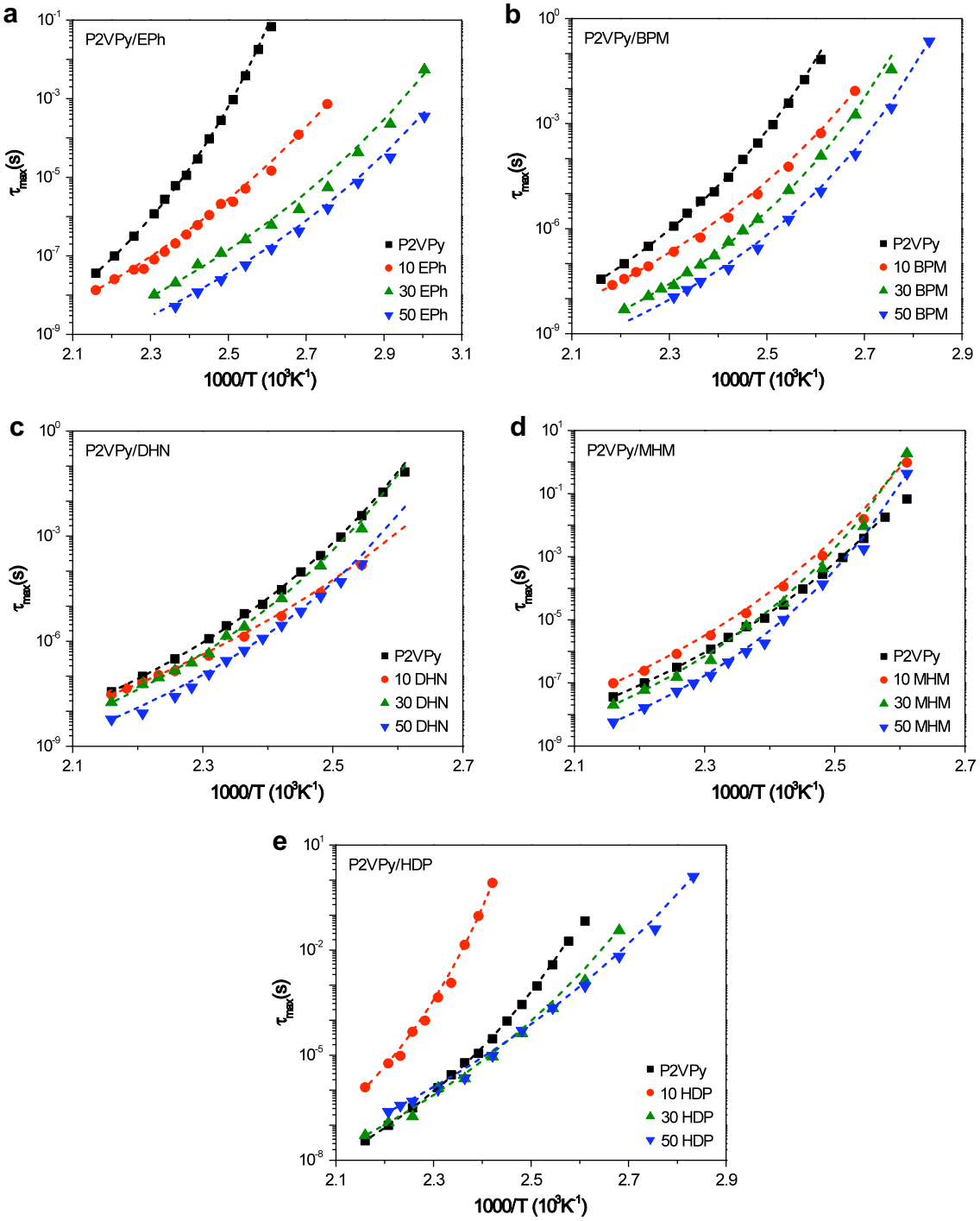

Fig. 6. Relaxation times of the α process as a function of temperature for P2VPy and all mixtures. Dashed lines indicate VFT fits.

conductivity (S/cm); ω is the angular frequency; τ_{HN} is the characteristic relaxation time; and m and n are shape parameters, indicative of the breadth of the relaxation and peak asymmetry, respectively. The exponent s characterizes the conduction process.

In some circumstances, dielectric constants were transformed into the dielectric loss factor via a numerical version of the Kramers–Kronig (KK) transform [37,38]:

$$\varepsilon''_{KK}(\omega) = \sum_{k=1}^{4} a_k \left[\varepsilon'\left(\frac{\omega}{2^k}\right) - \varepsilon'\left(\frac{2^k}{\omega}\right) \right] \quad (2)$$

The KK transform used here utilizes an 8-point numerical method and the coefficients developed by Steeman and van Turnhout [38].

3. Results and discussion

3.1. Glass transition behavior

A single T_g was observed for all P2VPy mixtures suggesting that mixing is relatively homogeneous. T_gs determined directly from DSC were very similar to those estimated from DRS using

VFT parameters ($T_g^{DRS} = T_{ref}$) [28], as shown in Fig. 2. Experimental T_gs follow predictions from the classic but rather restrictive Fox equation [39] surprisingly well, particularly considering the approximate values of the small molecule T_gs. The only exception is P2VPy–10 mol% HDP: this blend displays a T_g much higher (129 °C) than those of neat P2VPy (107 °C) and HDP (~28 °C). This is most probably due to complex formation that is a result of strong intermolecular hydrogen bonding, as observed previously for poly(4-vinylphenol)–P2VPy complexes [5,14]. In hydrogen-bonded systems, this type of S-shaped T_g/composition curve has been shown to be a result of a balance between self-association (i.e., OH–OH hydrogen bonds) and inter-association terms (OH–N hydrogen bonds). Why the 30% and 50% HDP mixtures behave differently is unclear at present, but it is well known that complex formation is sensitive to preparation conditions [16]. For clarity, the P2VPy/HDP mixtures are generally discussed separately later in this paper.

3.2. Hydrogen bonding

3.2.1. FTIR

FTIR spectroscopy was used to characterize the type and strength of hydrogen bonding between the components of the mixtures through an examination of the OH stretching region of the spectrum between 3600 cm^{-1} and 2400 cm^{-1}, as shown in Fig. 3. The spectra of the pure phenolics are complex in their own right, with even the simplest phenolic, EPh, displaying a number of broad overlapping bands in this region of the spectrum (Fig. 3a) [40,41]. However, in terms of what we need to consider here, the most important observation is that in simple phenolics the strongest band is observed near 3330 cm^{-1} and is characteristic of phenolic OH groups hydrogen bonded to one another in the form of chains [41,42]. The spectra of BPM are similar (Fig. 3b), but the OH stretching band in dihydroxynaphthalene, DHN, is observed at somewhat lower wavenumber (~3250 cm^{-1}, Fig. 3c), with a noticeable asymmetric broadening on the high wavenumber side. The shift to lower frequency indicates that there are hydrogen bonds in this phenolic that are stronger than those found in EPh, but these are just one component of a distribution that also includes weaker hydrogen-bonded groups. The spectrum of MHM, a molecule that essentially has four cresol molecules linked by methylene groups, also displays a similar, strongly hydrogen-bonded OH stretching mode (Fig. 3d). These types of molecules form calixarene-like structures with strong intramolecular hydrogen bonds that result in a band near 3250 cm^{-1} [42]. Finally, HDP, which contains three OH groups on each aromatic ring, displays a prominent band centered near 3150 cm^{-1}, as shown in Fig. 3e, presumably as a result of the formation of some very strongly hydrogen-bonded complex.

When mixtures of these phenolic molecules with P2VPy are formed, some of the phenolic OH–OH hydrogen bonds are replaced by OH–N hydrogen bonds to an extent that depends upon composition. The latter hydrogen bonds are very strong and the OH stretching mode shifts to near 3000 cm^{-1}, where it overlaps with the CH stretching modes of P2VPy [40], as can be seen in the spectra shown in Fig. 3a–e. These intermolecular hydrogen bonds are so strong that in ethyl phenol/P2VPy mixtures, essentially all the OH–OH hydrogen bonds are replaced by OH–N hydrogen bonds, even in those mixtures with the highest concentration of EPh (50%). In BPM/P2VPy blends, however, some OH–OH hydrogen-bonded groups become apparent as the concentration of this phenolic in the mixtures is increased. As might be expected, in the spectra of the remaining phenolic/P2VPy blends, where the OH–OH hydrogen bonds are stronger, the equilibrium distribution of OH–OH and OH–N hydrogen bonds is different, with some OH–OH hydrogen bonds being apparent, even in the spectra of the 10% phenolic/P2VPy mixtures. Interestingly, most of these OH–OH hydrogen bonds are weaker than those found in the pure phenolic parent materials, with broad bands centered near 3350 or 3400 cm^{-1}, similar to the OH band profile of neat EPh. The exception to this appears to be P2VPy/HDP mixtures, which we will discuss in more detail below, but in general it appears that the formation of complexes or structures with strong OH–OH hydrogen bonds is inhibited in the presence of P2VPy.

3.2.2. WAXD

Fig. 4 displays the X-ray diffraction patterns for 10 and 50 mol% solutions of the small molecules in P2VPy (diffraction patterns from the 30% mixtures are similar). The absence of crystalline diffraction peaks indicates that the small molecules are relatively well dispersed in the host polymer. Two amorphous halos were observed for neat P2VPy, and the lower angle halo has been assigned to arise from the mean intermolecular distance between the chains and the second to either the mean interpendant or intrapendant group distance [43–46]. The peak intensity of the higher angle halo has been found to be more prominent compared to the lower angle halo for polymers containing phenyl pendant groups such as polystyrene and its derivative [30,31,47], as well as P2VPy and P4VPy [43,44,48]. This is due to the more ordered-glassy structures when the intra-phenyl interactions between intrachain and interchain phenyl groups are present. The location of the amorphous halos remains approximately the same for all mixtures in this study.

3.2.3. SAXS

No scattering maximum was observed for any of the P2VPy/EPh, P2VPy/BPM, P2VPy/DHN and P2VPy/MHM solutions (Fig. 5), indicating no discernable microphase separation at the length scales ranging from 5 to 40 nm.

3.3. Dielectric relaxation of mixtures

3.3.1. Segmental relaxations

Fig. 6 presents the relaxation times τ_{max} of the segmental α processes as a function of temperature for five mixtures under consideration. The relaxation times of all samples are well fit by the Vogel–Fulcher–Tammann (VFT) relation [49], with τ_0 fixed at 10^{-14} s. The fitting parameters B and T_0 are provided in Table 2.

Table 2
VFT fit parameters for P2VPy and all mixtures.

Sample	VFT parameters	
	T_0 (°C)	B (eV)
P2VPy	22	0.22
10 EPh	−39	0.28
30 EPh	−47	0.24
50 EPh	−47	0.22
10 BPM	2	0.23
30 BPM	19	0.18
50 BPM	14	0.17
10 DHN	2	0.24
30 DHN	34	0.18
50 DHN	36	0.19
10 MHM	31	0.22
30 MHM	47	0.18
50 MHM	51	0.16
10 HDP	71	0.19
30 HDP	−2	0.25
50 HDP	−30	0.30

3.3.1.1. P2VPy/EPh. The segmental relaxation times of all three P2VPy/EPh solutions are faster than that of neat P2VPy and increase with increasing EPh concentration. The breadth of the segmental relaxation time distribution of P2VPy/EPh remains the same as neat P2VPy (Fig. 7a, for $T - T_g = 40$ °C). The slight broadening at high frequencies is due to the low-frequency tail of the local β relaxation process. The same behavior has been observed for mixtures of PVME with EPh, and was attributed to the absence of interchain cooperativity in the small molecule portion of the mixture and the promotion of a homogeneous environment encouraged by intermolecular hydrogen bonding between P2VPy and EPh [12]. The relaxation strengths for the fitted α processes were unusually variable and so are not provided in this paper. The relaxation strength for neat P2VPy was found to vary from approximately 12 at 110 °C–7.5 at 150 °C, in keeping with previous measurements [14].

3.3.1.2. P2VPy/BPM, P2VPy/DHN and P2VPy/MHM mixtures. Relaxation times of P2VPy/BMP are faster than that of neat P2VPy. Those for P2VPy/DHN are almost the same as neat P2VPy for 10 and 30 mol%, and become slightly faster at 50 mol%. The α process for P2VPy/MHM at 10 mol% is slightly slower than neat P2VPy, almost the same at 30 mol% and becomes slightly faster at 50 mol% (Fig. 6). This behavior is consistent with results from DSC experiments discussed earlier. Moreover, the breadths of the α relaxations of P2VPy/BPM, P2VPy/DHN and P2VPy/MHM mixtures increase with concentration of the low molecular weight diluents and are broader than for neat P2VPy, particularly at 30 and 50 mol%, as seen in Figs. 7 and 8. Therefore in

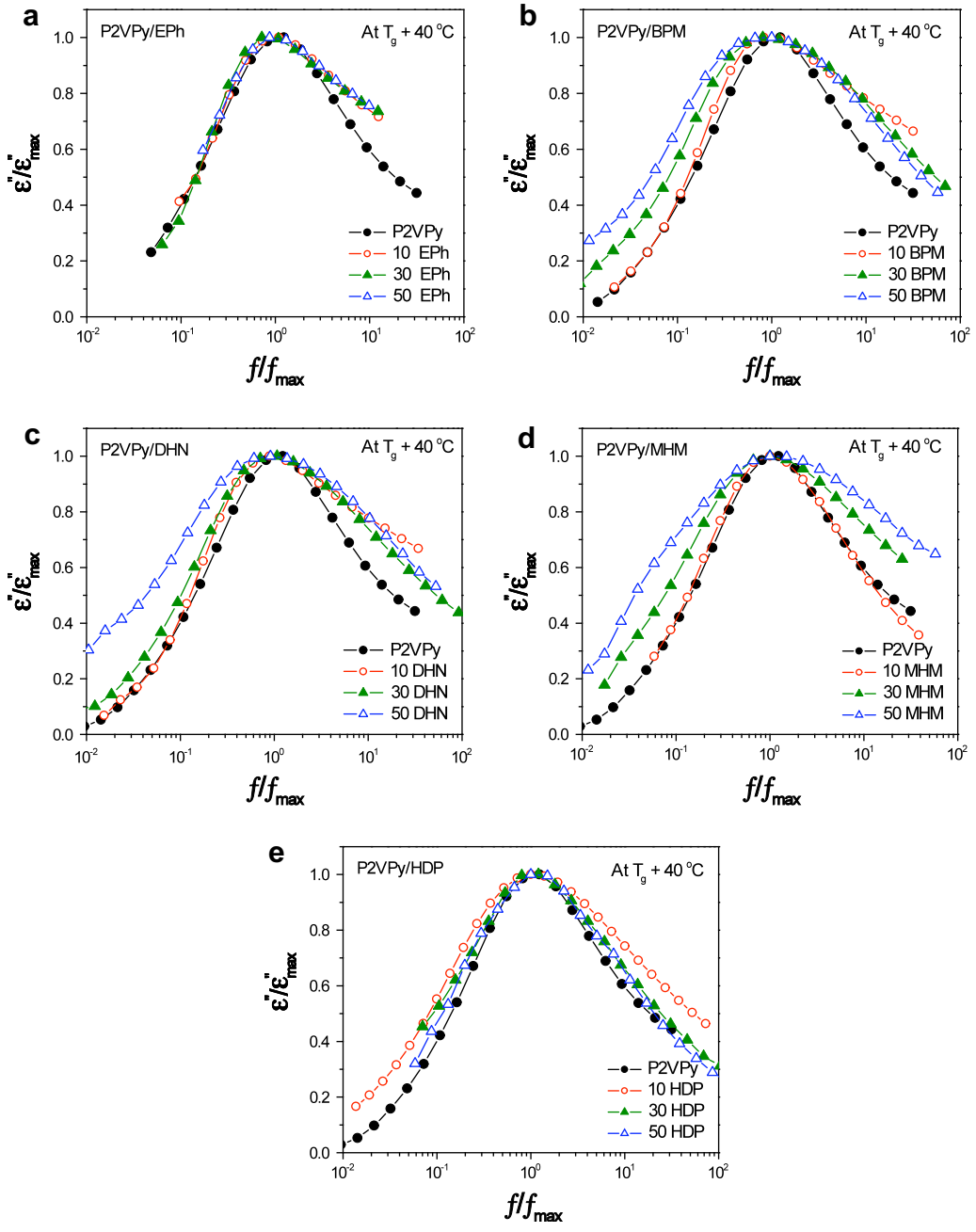

Fig. 7. Normalized segmental loss of (a) P2VPy/EPh, (b) P2VPy/BPM, (c) P2VPy/DHN, (d) P2VPy/MHM and (e) P2VPy/HDP at $T_g + 40$ °C.

contrast with P2VPy/EPh, this suggests that BPM, DHN and MHM solutions in P2VPy at concentrations above 10 mol% exhibit some degree of dynamic heterogeneity [10,11].

3.3.2. Local β relaxations

P2VPy exhibits a strong and broad local relaxation due to the rotation of pyridine side groups [48]. Fig. 9 presents the dielectric loss spectra for some selected solutions at −20 °C, normalized by the concentration of P2VPy in the solutions. The normalized strength of the β process decreases significantly with increasing diluent concentration, with the exception of the 30 and 50% EPh solutions for which the strengths appear to increase substantially (Fig. 10). We will return to the apparently anomalous behavior of the EPh solutions in the next paragraph. Fig. 10 shows that $\Delta\varepsilon(\beta)$ is strongly suppressed by the addition of DHN, BPM, MHM, HDP. In fact, the β relaxation is completely suppressed for the 50 mol% BPM and DHN solutions, and the 30 and 50 mol% MHM and HDP solutions. As seen for P2VPy blends with poly(vinyl phenol) [14], strong intermolecular hydrogen bonding results in suppression of the local rotations of the pyridine groups responsible for the β relaxation of P2VPy. Such suppression can have important ramifications to the mechanical properties, physical aging, and permeability in the glassy state as noted in the Introduction. In addition, the presence of two or more hydroxyl groups per diluent molecule may lead to the formation of transient crosslinks between chains.

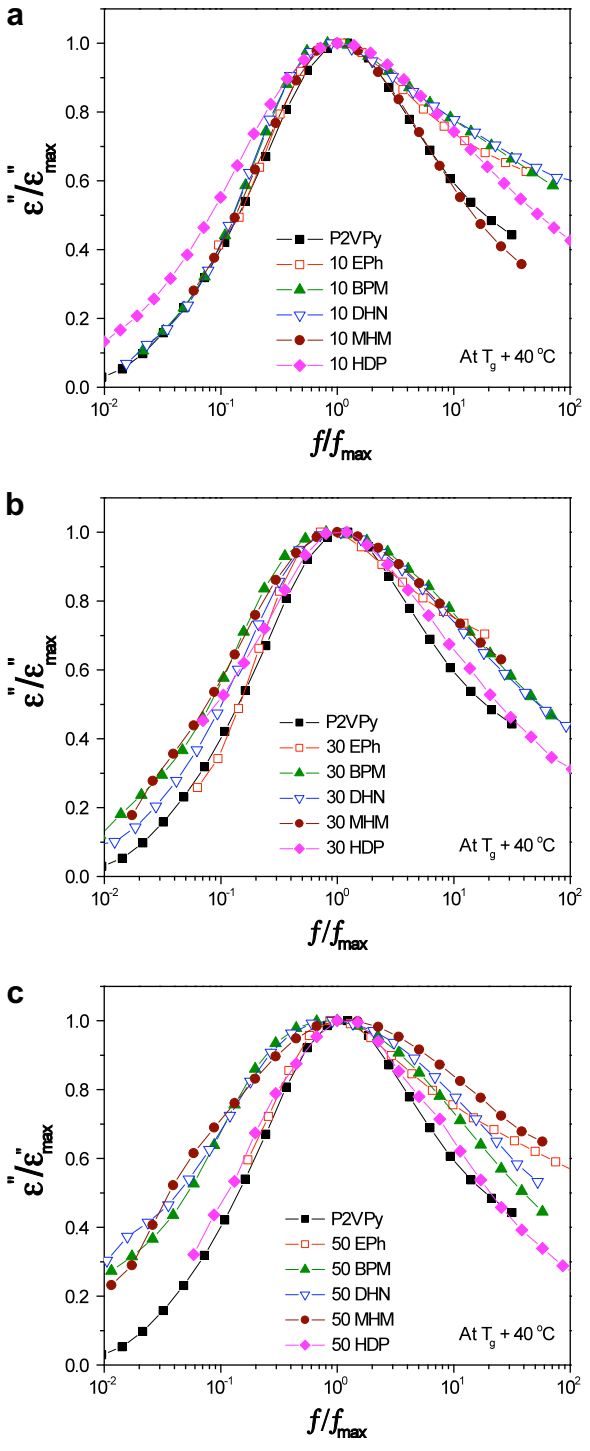

Fig. 8. Normalized segmental loss for mixtures with (a) 10 mol%, (b) 30 mol% and (c) 50 mol% of EPh, BPM, DHN, MHM and HDP at $T_g + 40$ °C.

Returning to the EPh mixtures, Fig. 10a shows that $\Delta\varepsilon(\beta)$ for the 30 and 50 mol% solutions appears to increase significantly with temperature. To develop an understanding of the origin of this, the dielectric relaxation behavior of neat EPh was measured, for the first time to the authors' knowledge. At temperatures below the T_g of EPh, neat EPh exhibits a very strong local relaxation (Fig. 11a), which can be compared with previous findings for isoeugenol (which has a structure similar to EPh) in which a similar transition was assigned to a Johari–Goldstein (JG) relaxation [53]. The JG relaxation involves the entire molecule and behaves similarly to the α relaxation. Comparison of the dielectric loss of neat P2VPy and EPh with the 30 and 50 mol% EPh solutions is shown in Fig. 11b. This clearly demonstrates the overlap of the P2VPy local motion with the JG relaxation of neat EPh, leading to the increase in strength in the 30 and 50 mol% mixtures. Therefore the apparent increase in $\Delta\varepsilon(\beta)$ with temperature and EPh content is associated with the increasing contribution of EPh β process.

The relaxation times of the 'residual' P2VPy β processes follow the expected Arrhenius temperature dependence, as displayed in Fig. 12. The activation energies, $E_a(\beta)$, and relaxation strengths at −20 °C are provided in Table 3. $E_a(\beta)$ for all but the BPM solutions are significantly higher than that of neat P2VPy, consistent with the influence of intermolecular H-bonding. Why E_a of the remaining local processes of the 10 and 30% BPM solutions does not behave in the same fashion is unclear, but is perhaps associated with the relatively flexible carbon single bond linkage between the two BPM phenol groups (Fig. 1).

3.4. P2VPy/HDP mixtures

3.4.1. Structural and spectroscopic evidence

The 30 and 50% P2VPy/HDP solutions do not exhibit any SAXS scattering peaks in the q range interrogated, but exhibit a strong increase in intensity at low q (Fig. 5a), similar to what is observed for ion-containing polymers [50,51] and phase separated polyurethanes e.g. [52]. The upturn in scattering intensity at very small angles presumably arises from spatial heterogeneity induced by the presence of hydrogen bond complexes [21]. P2VPy/10HDP exhibits a small scattering peak at $q \approx 0.06$ Å^{-1}, which corresponds to a mean inter-domain spacing of ~10 nm (Fig. 5a). Hydrogen-bonded mixtures possessing strong hydrogen bond linkages have been reported to exhibit SAXS peaks indicative of phase separation [21]. Based on DMA and FTIR results to be discussed shortly, we propose that P2VPy/10HDP exhibits some degree of phase separation, possibly as a result of a competition involving the formation of different types of hydrogen-bonded complexes.

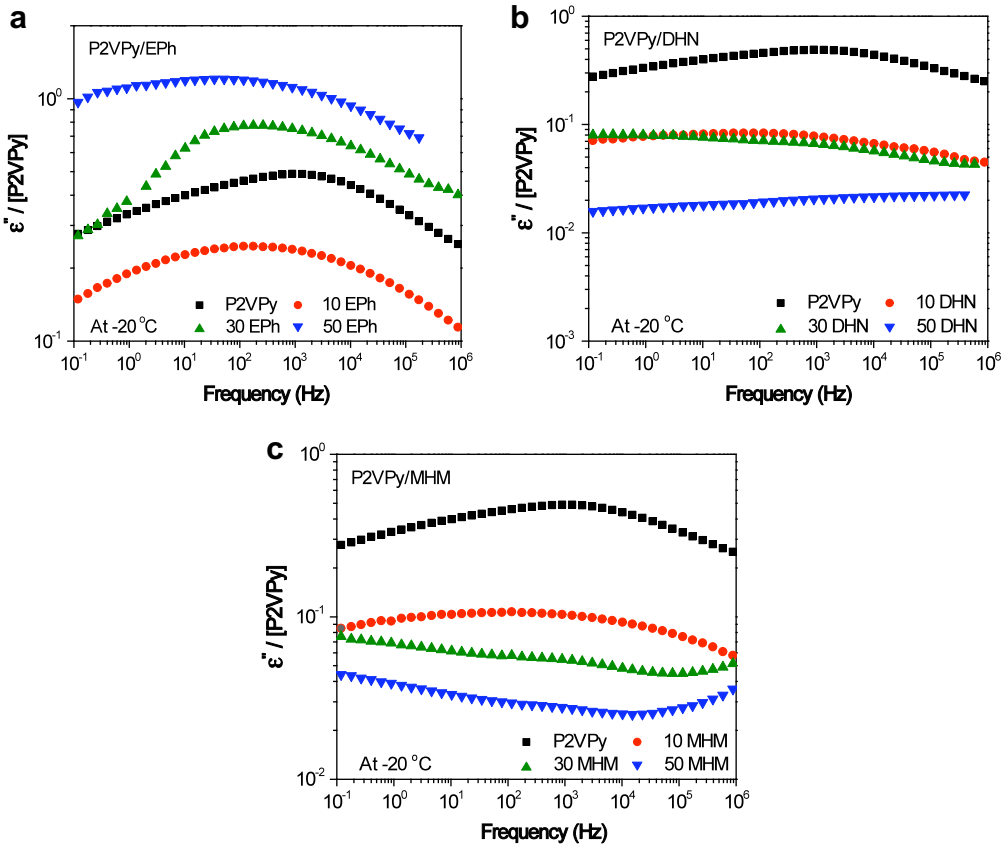

Fig. 9. Dielectric loss spectra normalized by P2VPy concentration at −20 °C for (a) P2VPy/EPh (b) P2VPy/DHN and (c) P2VPy/MHM at 10, 30 and 50 mol%.

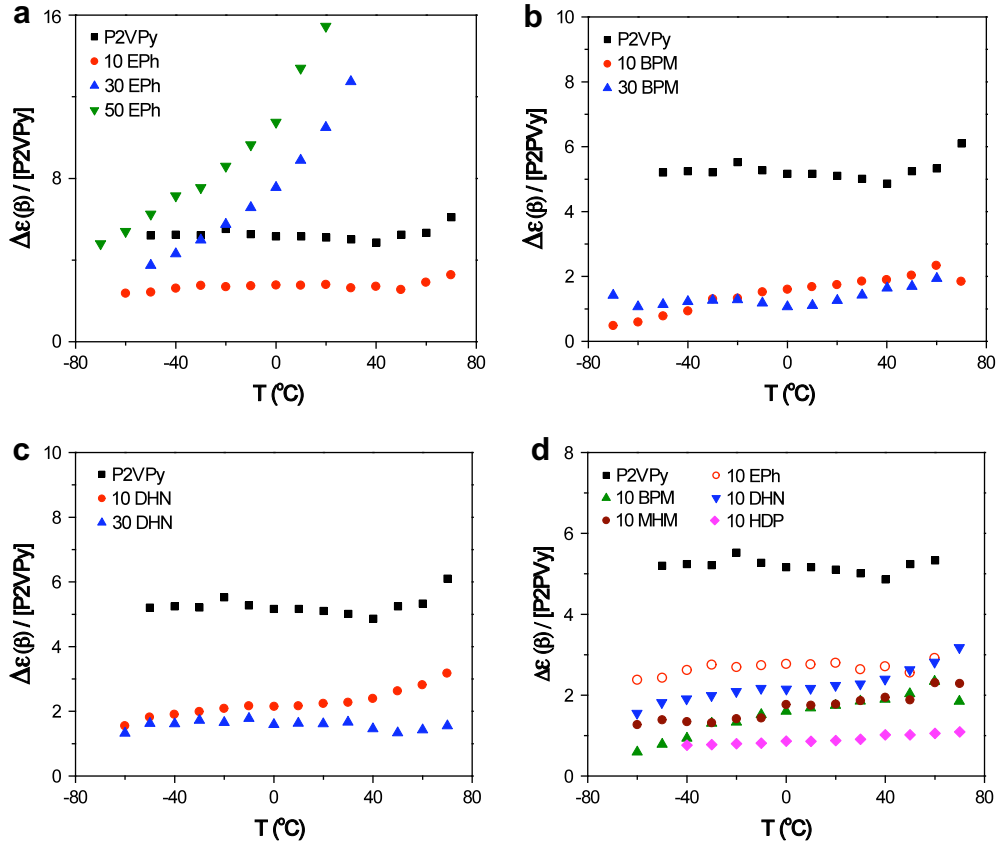

Fig. 10. Dielectric relaxation strengths for the β processes of (a) P2VPy/EPh at 10, 30 and 50 mol% EPh, (b) P2VPy/BPM at 10, 30 mol% BPM, (c) P2VPy/DHN at 10, 30 mol% DHN and (d) P2VPy with 10 mol% EPh, BPM, DHN, MHM and HDP.

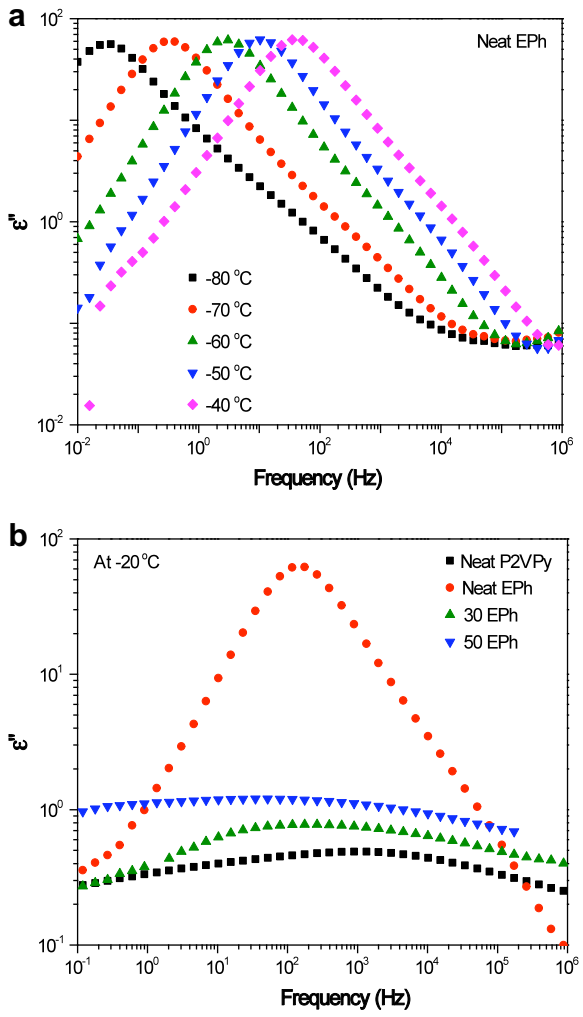

Fig. 11. Dielectric loss spectra for (a) neat EPh at selected temperature below −30 °C and (b) neat P2VPy compared to neat EPh, P2VPy mixed with 30 and 50 mol% EPh at −20 °C.

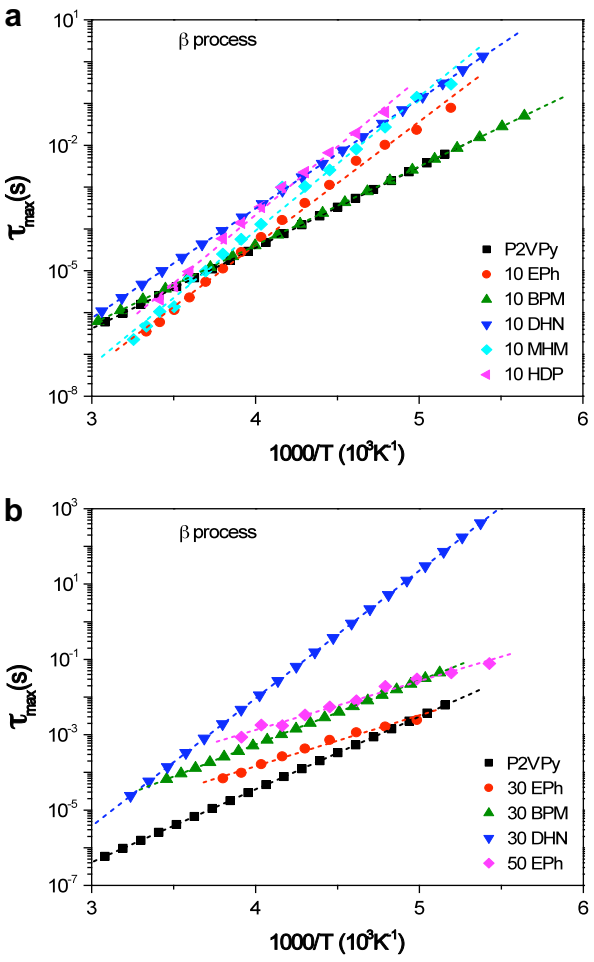

Fig. 12. (a) Temperature dependence of the β relaxation times of P2VPy and the mixtures. Dotted lines indicate Arrhenius fits.

Consistent with DSC observations, DMA results demonstrate that the mechanical α relaxation of P2VPy/10HDP is located at a higher temperature relative to neat P2VPy (Fig. 13). The presence of an extended rubbery plateau in E' suggests that P2VPy/10HDP imparts some physical crosslinking above T_g in this mixture. However no transitions above the α relaxation are observed.

The changes in hydrogen bonding as a function of composition in blends of P2VPy with HDP are somewhat different than in mixtures with other phenolics. This is a result of the unusually strong OH–OH hydrogen bonds that are formed between HDP molecules. As a result, even at low concentrations of HDP in the mixtures (10%), the band due to HDP hydrogen-bonded complexes near 3150 cm^{-1} is still present and overlaps a band near 3400 cm^{-1}, characteristic of the type of OH–OH hydrogen bonds found in simpler phenolics like EPh. As the concentration of HDP is increased, the formation of HDP/P2VPy hydrogen-bonded species appears to increase and the center of the very broad profile made up of various OH–OH and OH–N hydrogen-bonded species, shifts to lower frequencies. We suggest that the small scattering peak at $q \approx 0.06$ $Å^{-1}$ observed in the 10% mixtures of HDP with P2VPy is a result of a phase separation of different types of hydrogen-bonded complexes, one rich in P2VPy and the other involving the type of HDP hydrogen-bonded structures found in the pure state.

3.4.2. Dynamics of P2VPy/HDP

3.4.2.1. β process. The measured relaxation strengths provided in Fig. 10d demonstrate that the local glassy state process P2VPy/10HDP is strongly suppressed, and that of the 30 and 50 mol% HDP solutions is completely suppressed. $\Delta\varepsilon(\beta)$ for the 10% HDP solution is significantly lower than that of the other 10% solutions (Table 3), due to strong intermolecular hydrogen bonding, restricting the rotation of pyridine groups responsible for the β process.

3.4.2.2. α process. The 30 and 50 mol% HDP solutions exhibit segmental relaxation time behavior similar to that of the EPh, BPM, DHN and MHM solutions. However, consistent with the DSC results described earlier, P2VPy/10HDP relaxes much more slowly than neat P2VPy and the other mixtures (Fig. 6e). The segmental process of P2VPy/10HDP is slightly broader than that of neat P2VPy at $T_g + 40$ °C, while the normalized segment loss processes of the 30 and 50 mol% HDP solutions are unchanged from neat P2VPy (Fig. 7e).

3.4.2.3. α_2. Of the solutions under investigation here, P2VPy/10HDP is the only one to exhibit an additional process, α_2, at frequencies between α and the manifestation of electrode polarization, α_{EP} (Fig. 14). The α_2 relaxation emerges from the α process at 160 °C and moves to higher frequency with increasing temperature (see the inset in Fig. 14). As noted earlier, a slightly extended plateau in DMA and a rather high T_g suggest that P2VPy/10HDP contains

Table 3
β relaxation strength (normalized by the concentration of P2VPy) at −20 °C and activation energy of the P2VPy mixtures.

Sample	$E_a(\beta)$ (kJ/mol)	$\Delta\varepsilon(\beta)$/[P2VPy] at −20 °C
P2VPy	41	5.5
10 EPh	56	2.7
10 BPM	36	1.3
10 DHN	50	2.1
10 MHM	61	1.4
10 HDP	63	0.7
30 BPM	33	1.2
30 DHN	65	1.6

very strong intermolecular associations, perhaps even the formation of a complex. At first glance, it may seem reasonable to assign the α_2 process to the association and dissociation of a transient hydrogen-bonded stickers (α^*), as observed previously for SPS-H [28]. A feature important to the α^* processes of SPS and other H-bonded systems that facilitates its assignment, is that $\Delta\varepsilon(\alpha^*)$ decreases with increasing temperature, arising from the reduction in the number of transient hydrogen-bonded stickers [26,28,54]. However, the estimated increase in $\Delta\varepsilon(\alpha_2)$ with increasing temperature is not consistent with the assignment of this process to α^*. Instead, based on the SAXS scattering peak, we propose that the α_2 process is associated with Maxwell–Wagner–Sillars (MWS) interfacial polarization, arising from regions within the matrix with

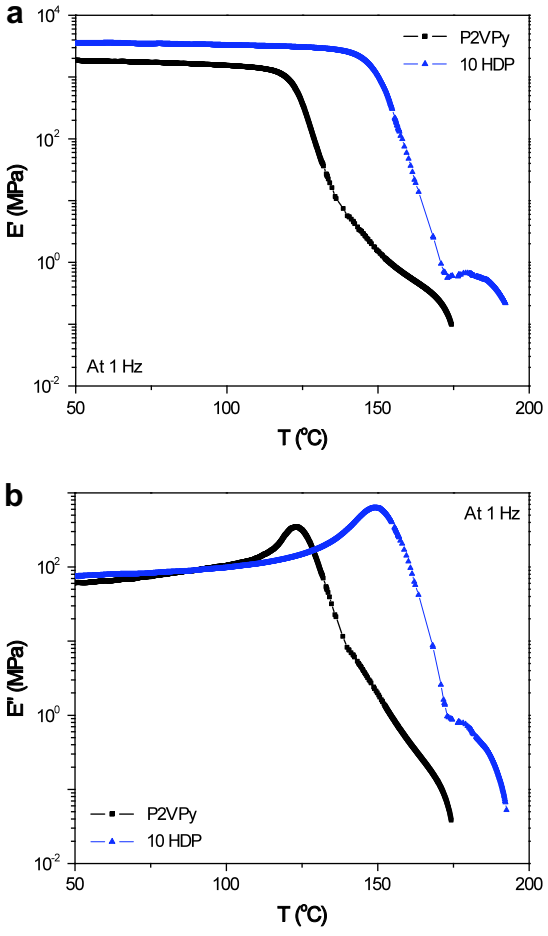

Fig. 13. Dynamic mechanical (a) storage and (b) loss modulus vs. temperature for P2VPy and P2VPy/10HDP at 1 Hz.

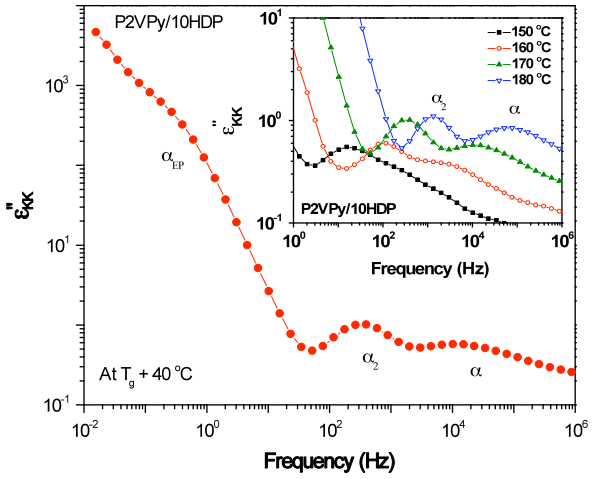

Fig. 14. ε''_{KK} spectrum vs. frequency for P2VPy/10HDP at $T_g + 40$ °C. Inset: ε''_{KK} spectra vs. frequency for P2VPy/10HDP at 150–180 °C.

different dielectric constant and conductivity [55]. A similar process has been previously observed in sulfonated polystyrene ionomers [56].

4. Summary

For all solutions except for P2VPy/10HDP, T_gs were found to more or less follow the predictions of the simple Fox equation. X-ray diffraction patterns exhibit only the two amorphous halos associated with P2VPy, with no evidence of small molecule crystallinity.

The significantly broadened dielectric α relaxation time distribution of P2VPy solutions with BPM, DHN and MHM at 30 and 50 mol% is attributed to dynamic heterogeneity, whereas P2VPy/EPh mixtures display dynamic homogeneity. P2VPy exhibits a strong and broad local relaxation due to the rotation of pyridine side groups. For all mixtures except 30 and 50% EPh where there is overlap of the P2VPy β process with the JG relaxation of EPh, the presence of small molecules containing multiple hydroxyl species significantly suppress the P2VPy β motion due to the formation of transient crosslinking, leading to a decrease in the number of free pyridine groups.

P2VPy/10HDP was the only mixture exhibiting a significantly higher T_g and T_α and a small SAXS scattering peak. An additional dielectric α_2 process was found at higher temperatures for P2VPy/10HDP, which we propose can be assigned to an MWS relaxation. We propose that this behavior is a result of a phase separation of different types of hydrogen-bonded complexes, one rich in P2VPy and the other involving the type of DHN hydrogen-bonded structures found in the neat state.

Acknowledgements

The authors would like to thank the National Science Foundation, Polymers Program (DMR-0605627), for support of this research.

References

[1] Utracki LA, Weiss RA. Multiphase polymers: blends and ionomers. Washington, DC: American Chemical Society; 1989.
[2] He Y, Zhu B, Inoue Y. Prog Polym Sci 2004;29:1021.
[3] Lee S, Lee JG, Lee H, Choe S. Macromolecules 1999;32:5961.
[4] Ahn T-K, Kim M, Choe S. Macromolecules 1997;30:3369.

[5] Painter PC, Graf JF, Coleman MM. Macromolecules 1991;24:5630.
[6] Coleman MM, Narvett LA, Painter PC. Polymer 1998;39:5867.
[7] Coleman MM, Guigley KS, Painter PC. Macromol Chem Phys 1999;200:1167.
[8] Motzer HR, Painter PC, Coleman MM. Macromolecules 2001;34:8390.
[9] Shinyashiki N, Imoto D, Yagihara S. J Phys Chem 2007;111:2181.
[10] Zhang SH, Painter PC, Runt J. Macromolecules 2002;35:9403.
[11] Zhang SH, Jin X, Painter PC, Runt J. Macromolecules 2002;35:3636.
[12] Zhang SH, Jin X, Painter PC, Runt J. Macromolecules 2003;36:7179.
[13] Zhang SH, Jin X, Painter PC, Runt J. Polymer 2004;45:3933.
[14] Zhang SH, Painter PC, Runt J. Macromolecules 2004;37:2636.
[15] Jin X, Zhang SH, Horvath JR, Runt J. J Phys Chem B 2004;108:7681.
[16] Riedel P, Kumpfer JR, Rogness DC, Wiegel KN. J App Polym Sci 2006;102:5890.
[17] Wubbenhorst M, Turnhout JV, Folmer BJB, Sijbesma RP, Meijer EW. IEEE Trans Dielectr Electr Insul 2001;8:365.
[18] He C, Donald A, Griffin A, Waigh T, Windle A. J Polym Sci Part B Polym Phys 1998;36:1617.
[19] Seidel U, Hilger C, Hellmann J, Schollmeyer D, Stadler R. Supramol Sci 1995;2:45.
[20] Hilger C, Drager M, Stadler R. Macromolecules 1992;25:2498.
[21] Hilger C, Stadler R. Macromolecules 1992;25:6670.
[22] Takano A, Kawashima W, Noro A, Isono Y, Tanaka N, Dotera T, et al. J Polym Sci Part B Polym Phys 2005;43:2427.
[23] Rittigstein P, Priestley RD, Broadbelt LJ, Torkelson JM. Nat Mater 2007;6:278.
[24] Priestley RD, Rittigstein P, Broadbelt LJ, Fukao K, Torkelson JM. J Phys Condens Mater 2007;19:205120.
[25] Anopchenko A, Psurek T, VanderHart D, Douglas JF, Obrzut J. Phys Rev E 2006;74:031501.
[26] Muller M, Stadle R, Kremer F, Williams G. Macromolecules 1995;28:6942.
[27] Muller M, Dardin A, Seidel U, Balsamo V, Ivan B, Spiess W, et al. Macromolecules 1996;29:2577.
[28] Atorngitjawat P, Klein RJ, Runt J. Macromolecules 2006;39:1815.
[29] Andreeva D, Ip B, Gurinov AA, Tolstoy PM, Denisov GS, Shenderovich IG, et al. J Phys Chem A 2006;110:10872.
[30] Fernandez-Berridi MJ, Iruin JJ, Irusta L, Mercero JM, Ugalde JM. J Phys Chem A 2002;106:4187.
[31] Topouza D, Orfanou K, Pispas S. J Polym Sci Part A Polym Chem 2004;42:6230.
[32] Zhang W, Shi L, Gao L, An Y, Wu K. Macromol Rapid Commun 2005;26:1341.
[33] Frisch MJ, Trucks GW, Schlegel HB, Scuseria GE, Robb MA, Cheeseman JR, et al. Gaussian 03. Revision E.01. Wallingford, CT: Gaussian, Inc.; 2004.
[34] McClellan AL. Tables of experimental dipole moments, vol. 2. El Cerrito, CA: Rahara Enterprises; 1974.
[35] McClellan AL. Tables of experimental dipoles moments, vol. 3. El Cerrito, CA: Rahara Enterprises; 1989.
[36] Havriliak S, Negami S. J Polym Sci Polym Symp 1966;14:99.
[37] Wubbenhorst M, vanTurnhout J. J Non-Cryst Solids 2002;305:40.
[38] Steeman PAM, van Turnhout J. Colloid Polym Sci 1997;275:106.
[39] Painter PC, Coleman MM. Fundamentals of polymer science: an introductory text. Florida: CRC Press; 1997. p. 303.
[40] Coleman MM, Graf JF, Painter PC. Specific interactions and the miscibility of polymer blends. PA: Technomic Publishing; 1991.
[41] Choperena A, Painter P.C. Vibrational Spectrosc, submitted for publication.
[42] Opaprakasit P, Scaroni A, Painter PC. J Mol Struct 2001;570:25.
[43] Kuo S-W, Wu C-H, Chang F-C. Macromolecules 2004;37:192.
[44] Choi S, Kim JH, Kang YS. Macromolecules 2001;34:9087.
[45] Aguilar-Vega M, Paul DR. J Polym Sci Part B Polym Phys 1993;31:1577.
[46] Mitchell GR, Windle AH. Polymer 1984;25:906.
[47] Floudas G, Pakula T, Stamm M, Fischer EW. Macromolecules 1993;26:1671.
[48] Papadopoulos P, Peristeraki D, Floudas G, Koutalas G, Hadjichristidis N. Macromolecules 2004;37:8116.
[49] Angell CA. Polymer 1997;38:6261.
[50] Fragiadakis D, Dou S, Colby RH, Runt J. Macromolecules 2008;41:5723.
[51] Wu DQ, Phillips JC, Lundberg RD, Macknight WJ. Macromolecules 1989;22:992.
[52] Garrett JT, Lin JS, Runt J. Macromolecules 2000;33:6353.
[53] Kamiska E, Kaminski K, Paluch M, Ngai KL. J Chem Phys 2006;124:164511.
[54] Muller M, Kremer F, Stadler R, Fischer EW, Seidel U. Colloid Polym Sci 1995;273:38.
[55] Weiss RA, Sen A, Willis CL, Pottick LA. Polymer 1991;32:1867.
[56] Atorngitjawat P, Runt J. Macromolecules 2007;40:991.